HHS Public Access

Author manuscript

Biomaterials. Author manuscript; available in PMC 2022 January 25.

Published in final edited form as:

Biomaterials. 2020 July ; 245: 119978. doi:10.1016/j.biomaterials.2020.119978.

The Effect of a Nanofiber-Hydrogel Composite on Neural Tissue Repair and Regeneration in the Contused Spinal Cord

Xiaowei Li[a,b,c,†,#], **Chi Zhang**[a,b,c,d,†], **Agnes E. Haggerty**[e,†], **Jerry Yan**[a,c,f], **Michael Lan**[a,c,f], **Michelle Seu**[a,g], **Mingyu Yang**[a,b,c], **Megan M. Marlow**[e], **Inés Maldonado-Lasunción**[e,h,i,j,k], **Brian Cho**[a,g], **Zhengbing Zhou**[a,b,c], **Long Chen**[a,b,c], **Russell Martin**[a,b,c], **Yohshiro Nitobe**[e,l], **Kentaro Yamane**[e,m], **Hua You**[n], **Sashank Reddy**[g], **Da-Ping Quan**[d,*], **Martin Oudega**[i,j,k,n,o,*], **Hai-Quan Mao**[a,b,c,f,*]

[a]Translational Tissue Engineering Center, Johns Hopkins University, Baltimore, MD 21205, USA

[b]Department of Materials Science & Engineering, Johns Hopkins University, Baltimore, MD 21205, USA

[c]Institute for NanoBioTechnology, Johns Hopkins University, Baltimore, MD 21205, USA

[d]School of Chemistry, Sun Yat-Sen University, Guangzhou, Guangdong 510275, P. R. China

[e]The Miami Project to Cure Paralysis, University of Miami, Miami, FL 33136, USA

[f]Department of Biomedical Engineering, Johns Hopkins University, Baltimore, MD 21205, USA

[g]Department of Plastic and Reconstructive Surgery, Johns Hopkins School of Medicine, Baltimore, MD 21287, USA

[*]Corresponding Authors: H.-Q. Mao: 100 Croft Hall, 3400 N. Charles Street, Baltimore, MD 21205, USA.; hmao@jhu.edu, M. Oudega: 355 E Erie St., Shirley Ryan AbilityLab, Chicago, IL 60611, USA, moudega@sralab.org, D.-P. Quan: 135 W. Xinggang Road, Guangzhou, Guangdong 510275, P. R. China, cesqdp@mail.sysu.ed.cn.

[#]Current address: Mary and Dick Holland Regenerative Medicine Program, Department of Neurological Sciences, University of Nebraska Medical Center, NE 68198, USA

[†]These authors contributed equally to this work.

Author contributions

X.L., C.Z., H.Y., and A.E.H. contributed to the design, execution, and analysis of the experiments. A.E.H., M.M.M., I.M., Y.N., and K.Y. performed all spinal cord contusions, injections, and dissections. J.Y., M.S., M.L., and M.Y. cut the tissue and performed staining. A.E.H., H.Y. B.C., R.M., S.R., L.C., Z.Z., and D.-P.Q. contributed to the discussion of the experimental design and interpretation of results. H.-Q.M. and M.O. conceived the project and contributed to the study design and result analysis. X.L., A.E.H., M.O., and H.-Q.M. prepared the manuscript with inputs from all authors.

Competing financial interests

H.-Q.M., S.R., and R.M. are co-founders of LifeSprout LLC, a startup company that has licensed the technology described in this manuscript.

Data and materials availability

All data and materials described in this manuscript are available.

Appendix A. Supplementary data

Supplementary data to this article can be found online.

Declaration of interests

The authors declare that they have no known competing financial interests or personal relationships that could have appeared to influence the work reported in this paper.

[h]Department of Regeneration of Sensorimotor Systems, Netherlands Institute for Neuroscience, Institute of the Royal Netherlands Academy of Arts and Sciences, Amsterdam, The Netherlands

[i]Shirley Ryan AbilityLab, Chicago, IL 60611, USA

[j]Department of Physical Therapy and Human Movements Sciences, Chicago, IL 60611, USA

[k]Department of Physiology Northwestern University, Chicago, IL 60611, USA

[l]Department of Orthopedic Surgery, Hirosaki University Graduate School of Medicine, Hirosaki, Aomori, 036-8562, Japan

[m]Department of Orthopedic Surgery, Okayama University Graduate School of Medicine, Dentistry, and Pharmaceutical Science, Kitaku, Okayama 700-8558, Japan

[n]Affiliated Cancer Hospital, Guangzhou Medical University, Guangzhou, Guangdong 510095, P. R. China

[o]Edward Hines Jr. VA hospital, Hines IL 60141, USA.

Abstract

An injury to the spinal cord causes long-lasting loss of nervous tissue because endogenous nervous tissue repair and regeneration at the site of injury is limited. We engineered an injectable nanofiber-hydrogel composite (NHC) with interfacial bonding to provide mechanical strength and porosity and examined its effect on repair and neural tissue regeneration in an adult rat model of spinal cord contusion. At 28 days after treatment with NHC, the width of the contused spinal cord segment was 2-fold larger than in controls. With NHC treatment, tissue in the injury had a 2-fold higher M2/M1 macrophage ratio, 5-fold higher blood vessel density, 2.6-fold higher immature neuron presence, 2.4-fold higher axon density, and a similar glial scar presence compared with controls. However, the spared nervous tissue volume in the contused segment and hind limb function was similar between groups. Our findings indicated that NHC provided mechanical support to the contused spinal cord and supported pro-regenerative macrophage polarization, angiogenesis, axon growth, and neurogenesis in the injured tissue without any exogenous factors or cells. These results motivate further optimization NHC and delivery protocol to fully translate the potential of the unique properties of NHC for treating spinal cord injury.

Keywords

Nanofiber; Hydrogel; Composite; Spinal cord injury; Angiogenesis; Macrophage polarization; Axonal growth; Neurogenesis

1. Introduction

A contusion to the spinal cord results in nervous tissue loss, which is typically long-lasting because endogenous events fail to elicit nervous tissue repair and/or generation, resulting in poor clinical prospects [1]. In time, a cystic cavity bordered by glial scar [2–5] develops in the contused segment, which in time collapses, posing formidable obstacles for nervous tissue repair and generation. The search for treatments that facilitate nervous tissue formation and repair in the contused spinal cord is ongoing [6].

The use of injectable hydrogels represents a particularly promising avenue for treatment of the contused spinal cord, as they can effectively fill the lesion cavity, thereby allowing for increased compatibility between the hydrogel and native tissue [7–10]. Also, hydrogels can imitate biological features of native extracellular matrix (ECM) [4, 7, 8], which may facilitate tissue regeneration and repair. Previous studies showed that hydrogels, including self-assembling RADA16-based peptide hydrogel [11], peptide amphiphile hydrogel [12], hyaluronic acid (HA) hydrogel [5, 7, 8, 10], poly(organophosphazenes) hydrogel [13], poly(N-[2-hydroxypropyl]-methacrylamide) hydrogel [14], and poly(2-hydroxyethylmethacrylate) hydrogel [15–17], could serve as a scaffold for axonal growth, albeit often to a limited extent [12].

After a contusion, the spinal cord typically collapses at the injury epicenter. A hydrogel that upholds the integrity of the contused segment may limit spinal cord collapse. An important design consideration in the development of mechanical-supporting hydrogels exists in achieving a close match between the mechanical properties of the hydrogel and native spinal cord nervous tissue, which has a shear storage modulus (G') on the order of 50 to 600 Pa [18, 19]. When replicating the properties of nervous tissue, one challenge of hydrogel design lies in the difficulty of decoupling mechanical strength from permeability. Although increasing the G' will impart mechanical integrity to the hydrogel, the necessary trade-off exists in a decrease in both the hydrogel's nutrient permeability and cell permeability.

To address these conflicting design constraints, we have developed a novel nanofiber-hydrogel composite (NHC) which mimics the microarchitecture and mechanical properties of soft tissue matrix [20]. In contrast to existing fiber-hydrogel blends, which primarily use physical mixing to combine the fibrous and hydrogel phases [21, 22], our composite relies on the interfacial bonding between the fibers and the hydrogel network. This unique bonding structure allows the composite to retain its shape and uphold the mechanical integrity of the injury site while simultaneously maintaining sufficient porosity to facilitate cellular migration within the matrix, thus establishing a cellular foundation for tissue regeneration and repair. The composite material consists of a thiol-modified HA hydrogel phase, which is covalently conjugated to fragmented, electrospun polycaprolactone (PCL) fibers. We utilized HA hydrogel, as HA is naturally distributed throughout the central nervous system and is biocompatible in the spinal cord [5, 8].

In the present study, we have adopted a clinically relevant adult rat model of spinal cord contusion to investigate the mechanical support of NHC and its effects on neural tissue generation by assessing the presence of macrophages, blood vessels, axons, and neural-like cells. We hypothesized that our composite material provides mechanical support to the contused spinal cord segment and provide a microenvironment that facilitates infiltration of endogenous cells, which is important for nervous tissue repair and generation.

2. Materials and methods

2.1. Ethics and surgical approval

Rats were housed according to the guidelines of the National Institutes of Health and the United States Department of Agriculture. All animal procedures were approved by the

Institutional Animal Care and Use Committee of the University of Miami. Before and after surgery, rats were kept in a double-barrier facility in standard cages with continuous fresh air and *ad libitum* water and food.

2.2. Study design

The spinal cord contusions and injections were performed at The Miami Project to Cure Paralysis at the University of Miami by personnel that were blinded to the treatments and experimental groups. Hind limb motor function testing was performed by members of the Animal Core Facility of The Miami Project to Cure Paralysis, which were blinded to the treatments and experimental groups. After dissection of the spinal cords, segments centered on the contusion were removed and shipped to Johns Hopkins University for histological processing, immunostaining, and analyses by personnel blinded to the treatments and experimental groups.

2.3. Materials

Thiolated hyaluronic acid (HA-SH, MW 250 kDa) and polyethylene glycol diacrylate (PEGDA, MW 3.4 kDa) were purchased from ESI BIO (Alameda, CA). All other chemical reagents were purchased from Sigma-Aldrich (St. Louis, MO).

2.4. Preparation of maleimide-modified PCL fibers

Poly(ε-caprolactone) (PCL) solution (16% w/w) was prepared in a mixture of dichloromethane and dimethylformamide (9/1 w/w). The green fluorescent dye, poly (9, 9-dioctylfluorene-alt-benzothiadiazole) (F8BT) was added to the PCL solution to enable detection of the fibers after injection. The PCL solution was electrospun to form PCL fibers.

Carboxyl groups were introduced to the surface of the PCL fibers using plasma surface activation [23] and converted to maleimide (MAL) groups through activation with ethyl dimethylaminopropyl carbodiimide and N-hydroxysuccinimide at a molar ratio of 1:4:4, respectively. N-(2-aminoethyl) MAL was added at a molar ratio of carboxyl groups to amine groups of 1:2 and the mixture was gently shaken to facilitate the conversion.

The MAL-modified PCL fibers were broken down into fragments with an average length of 44 to 67 μm using a cryogenic mill (Freezer/Mill 6770, SPEX SamplePrep, Metuchen, NJ) with a milling cycle number between 6 and 12 times (Fig. S1). These fragments were sterilized in three cycles of 70% v/v ethanol followed by distilled water. The resulting sterilized MAL-modified fiber fragments were lyophilized and stored at −20°C.

2.5. Preparation and rheological assessment of nanofiber-hydrogel composites and hydrogels

Nanofiber-hydrogel composites were prepared by mixing different amounts of MAL-fibers in HA-SH precursor solution with PEGDA. The composite was prepared with 10 mg/mL of MAL-fibers, 2 mg/mL of PEGDA, and 4 mg/mL of HA-SH in phosphate buffered saline (PBS). Hydrogels were prepared with 2 or 5 mg/mL of PEGDA and 4 mg/mL of HA-SH in PBS. We used a rheometer (ARG2, TA Instruments) to measure the G’ of the composite and hydrogels.

2.6. Spinal cord contusion and injection

Adult female Sprague Dawley rats (180–200 g, n = 107; Charles Rivers Laboratory, Wilmington, MA) were anaesthetized using an intraperitoneal injection of ketamine (60 mg/kg; Butlerschein, Dublin, OH) and dexmedetomidine (0.5 mg/kg; Pfizer, New York, NY). The ninth thoracic spinal cord level was contused using a force of 175 kDyne (Infinite Horizon IH-0400 impactor; Precision Systems and Instrumentation LLC, Versailles, KY) as described previously [24, 25]. Only rats that had an open field locomotor score ≤ 1 on the Basso-Beattie-Bresnahan (BBB) scale [26] at 1 day post-injury (dpi) were included in the experiments. Seven rats (6.5%) died during or within 24 h after surgery. For injection at 3 dpi, rats were anesthetized as described above and their contused spinal cord exposed. The injury epicenter was injected with 5 μL of NHC (G'= 210 Pa; n = 25), HA hydrogel-210 (G' = 210 Pa; n = 25), HA hydrogel-80 (G' = 80 Pa; n = 25), or phosphate-buffered saline (PBS, 0.1 M, pH 7.4; n = 25). We will refer to these four experimental groups as NHC, H-210, H-80, and PBS. All rats survived during and after the spinal cord injection until their designated time of fixation. From each experimental group, 15 rats were used to study anatomical and cellular changes in the injury/injection site at 3 (n = 5), 7 (n = 5), and 28 (n = 5) dpi and 10 rats to examine hind limb function for 56 dpi.

2.7. Post-surgery procedures and rat maintenance

After surgery, rats received a subcutaneous injection of Antisedan (1.5 mg/kg; Pfizer) to reverse the effects of dexmedetomidine [24, 25]. Starting directly after surgery, rats were treated with gentamicin (6 mg/kg, intramuscular; VWR) daily for 7 days and buprenorphine hydrochloride (1 mg/kg, subcutaneous; Reckitt Benckiser Pharmaceuticals, Inc., Richmond, VT, USA) twice daily for 3 days [24, 25]. In addition, rats received 10 mL Ringer's solution subcutaneously immediately after surgery and 5 mL daily for the next 3 days [24, 25]. Rats were housed in pairs during survival. The rats were maintained by professional caretakers blinded to the treatments and experimental groups. Bladders were manually emptied twice daily until reflex voiding started. Rats were cleaned and dried if needed. Rats were monitored daily throughout the study. None of the rats required treatment for pain or distress during survival.

2.8. ECM extraction from spinal cord

ECM was extracted from pig spinal cord [27]. Spinal cord tissue was decellularized using Triton X-100 (3%), sodium deoxycholate (4%), ethanol (4%), and sterile water at 4°C before freeze-drying and homogenization. Powdered homogenized tissue was digested in acidic solution containing pepsin for 12 h at 25°C before removal of any undigested particles through centrifugation at 30,000 rpm for 30 min. The pH was adjusted to 7.5 and the ionic strength to 0.15 M using PBS before being stored at −20°C.

2.9. Histological procedures

At designated times, rats were deeply anaesthetized using an intraperitoneal injection of ketamine (100 mg/kg; Butlerschein, Dublin, OH) and transcardially perfused with 300 mL PBS followed by 400 mL 4% paraformaldehyde in PBS. Spinal cords were dissected, post-fixed overnight in the same fixative, and transferred to 30% sucrose in PBS for 48

h. Images of representative spinal cords from each experimental group were taken under a dissection microscope. From the 5 spinal cords per time point per experimental group, a 12 mm-long segment centered on the contusion was removed, frozen, and cut on a cryostat into 12 series of 20 μm-thick horizontal (n = 3), 20 series of 10 μm-thick horizontal (n = 1), or 20 series of 10 μm-thick transverse (n = 1) sections. One of the 20 μm-thick horizontal cut spinal cords was used to test antibodies for immunostaining. Animals from which the spinal cord was cut into 10 μm-thick sections are denoted by an # next to the data point in the graphs. Note that the analyses were adjusted accordingly. Histological analyses were based on groups of three spinal cords.

2.10. Immunocytochemistry

For immunostaining, sections were permeabilized with 0.5% Triton X-100 in PBS, immune-blocked with 4% normal goat or donkey serum in PBS for 2 h, and then incubated with primary antibodies (Table S1) overnight at 4°C. After washing three times with PBS, sections were incubated for 2 hours with Cy5- or Cy3-conjugated secondary antibodies (1:200; Jackson ImmunoResearch Laboratories, Inc., West Grove, PA). Sections were washed three times with PBS, counterstained for 3 min at room temperature with the nuclear stain, DAPI (4',6-Diamidino-2-Phenylindole Dihydrochloride, 2 μL/mL; Thermo Fisher), and covered with glass slips in anti-fade fluorescent mounting medium (Dako). Sections were stored at 4°C until analysis under a Zeiss LSM 510 Meta Confocal Microscope (Thornwood, NY). Regions of Interest (ROIs) were selected for quantification from tile scans of 3.5 mm-long spinal cord segment centered on the contusion.

2.11. Determining the spinal cord width and volume of tissue in the injury

The width of the spinal cord was determined by measuring the side-to-side distance at the impact center in 3–6 sections spanning the injury in one series stained with anti-GFAP antibodies and counterstained with DAPI using Image J. The values were averaged per rat and per group and time. The injury was defined by the inner border of the GFAP-positive astrocytic scar present in the contused spinal cord segment. To determine the volume of tissue within the injury, the injury was outlined in 3–6 middle sections spanning the injury of one series at 28 dpi using ImageJ and the 460 nm (DAPI) filter. Volumes were determined by multiplying surface areas by the known distance between the middle section and by ½ of the known distance between the outer sections. Volumes were averaged across groups and presented as percentage of total injury volume.

2.12. Examination of inflammation in the injury

To assess inflammation, the numbers and phenotype of macrophages in the injury and in spinal cord tissue outside of the injury were determined in the 1–3 middle sections in one series per rat at 28 dpi using ImageJ. The injury border was defined by the inner border of GFAP staining. The tissue outside of the injury was defined as all tissue within 0.5 mm radially from the edge of the injury. Macrophages in general were recognized using antibodies against CD68, M1 macrophages using antibodies against CD86, and M2 macrophages using antibodies against CD206. Cells positive for each staining were counted and averaged per rat and per group. The acquired values were used to determine the M2/M1 macrophage ratios, which were averaged per rat and per group. In a series of cross-sections,

degree of co-localization of the nanofibers in the composite and M1 or M2 macrophages was visualized.

2.13. Assessment of vascularization in the injury

To determine the degree of vascularization, the number of RECA-1-positive blood vessels in the injury was measured in 1–4 middle sections in one series per rat at 3, 7, and 28 dpi using ImageJ with the Ridge Detection plug-in. The images were pre-processed by extracting the GFAP-defined injury and removing background pixels and static using ZEN software [28] followed by Ridge Detection plug-in with a minimum length of 18 μm. The number of blood vessels was expressed per surface area of the ROI. The acquired values were averaged per rat and per group and time.

2.14. Assessment of axons in the injury

To examine axon presence, the number of axons in the injury at 28 dpi was determined in 1–3 middle sections in one series per rat that was stained with antibodies against neurofilament protein H (high molecular weight, NF-H or NF) to recognize axons and against GFAP to recognize astrocytes. The latter was also used to define the injury ROI. ImageJ with the Ridge Detection plug-in was used to quantify axons within the GFAP-defined injury. Images were pre-processed by extracting the injury and removing background pixels and static using ZEN software [28] followed by ImageJ's Ridge Detection plug-in with a minimum length of 18 μm. The acquired values were averaged per rat and per group. The presence of astrocytes and their association with axons within the injury site was qualitatively assessed.

2.15. Neuron-like cells in the injury

We stained one series of sections with antibodies against βIII-tubulin (Tuj1) in immature neurons and neuronal processes and another series with antibodies against doublecortin (DCX) to recognize a microtubule-associated protein present in neuronal stem/progenitor cells. Tuj1-positive cells within the injury were quantified in 1–3 middle sections. Images were processed using ImageJ by first extracting the injury and removing background pixels and static using ZEN software [28] followed by ImageJ's Ridge Detection plug-in with a minimum length of 18 μm. Besides the number of cells, we also measured the length of Tuj1 positive processes. Each of the values were averaged per rat and per experimental group.

2.17. Additional tissue and behavioral analysis

The volume of nervous tissue outside of the injury and the GFAP-positive scar presence were determined. The BBB open field locomotor test [26] and horizontal ladder walking test [29] were used to assess hind limb motor function. The methods of these assessments are described in the Supplementary Data section.

2.18. Statistical analysis

Data are shown as mean ± standard deviation (SD) with individual data points overlaid on averages. Data were analyzed using nonparametric Kruskal-Wallis test (histological analysis) or repeated measures 2-way ANOVA (behavioral analysis). Values were considered significantly different at $p < 0.05$.

3. Results

We will first focus on the engineering aspects of the composite and its gross effects on the spinal cord after injection into the contusion. Next, we will provide a description of the cells and cellular structures in the injury. The injury is defined according to the method described for each of the analyses. Additionally, we have examined the nervous tissue (Fig. S2) and astrocytic scar (Fig. S3) in the contused spinal cord segment outside of the injury as well as hind limb motor function (Fig. S4).

3.1. Engineering a nanofiber-hydrogel composite with interfacial bonding

We engineered the injectable NHC by forming interfacial bonds between PCL nanofibers and HA molecules in the hydrogel phase (Fig. 1a). Scanning electron microscopy of the lyophilized composite revealed that the PCL fibers were connected to the HA hydrogel network through a fibrillary microarchitecture, resembling that seen in native spinal cord ECM (Fig. 1b).

To validate and quantitatively analyze interfacial bonding between PCL nanofibers and HA hydrogel, we determined the G' of composites with and without interfacial bonding. With 1% (w/w) nanofibers, the composite with interfacial bonding had a G' that was about 2-fold larger than that of the blend without interfacial bonding (Fig. 1c). The G' of the composite increases with increasing amounts of fibers (Fig. 1c). We were able to produce a composite with a G' of about 210 Pa, resembling that of spinal cord nervous tissue, while maintaining a hydrogel phase that is similar as that with a G' less than 100 Pa, which is adequately porous for cell infiltration [8, 30]. Based on these data we may expect that we engineered an injectable composite that provides mechanical support to a contused spinal cord segment while facilitating cell permeation.

3.2. Gross anatomy of the contused spinal cord segment

In all groups, at the site of impact, the spinal cord appeared to gradually decrease in width and develop a semitransparent appearance after impact (Fig. 2a). Quantification revealed that the width of spinal cords that received PBS or H-80 significantly decreases between 3 and 28 dpi (Fig. 2b; PBS: 1.9 ± 0.3 vs. 0.8 ± 0.2 mm, $p < 0.001$; H-80: 2.0 ± 0.3 vs. 1.1 ± 0.3 mm; $p < 0.01$). In contrast, the width of spinal cords injected with NHC or H-210 did not significantly decrease between 3 and 28 dpi. We found that the average width of the spinal cord at 28 dpi was 1.5 ± 0.4 mm with NHC, 1.6 ± 0.4 mm with H-210, 1.1 ± 0.3 mm with H-80, and 0.8 ± 0.2 mm with PBS (Fig. 2b). The width of NHC- and H-210-injected spinal cords at the contusion/injection site was about 2-fold larger ($p < 0.05$) than that of PBS-injected spinal cords at 28 dpi (Fig. 2b). Our results indicate that NHC significantly limited spinal cord thinning that is typically seen after a contusion.

The translucent appearance of the spinal cord at the site of impact is characteristic of a contusion injury and is due, at least in part, to the loss of nervous tissue and the formation of cavities. The translucent manifestation appeared less in spinal cords injected with NHC or HA than with PBS (Fig. 2a). In horizontal cryostat sections stained with antibodies against GFAP and counterstained with DAPI, we found cells/tissue present in the injury in

all groups (Fig. 2c). At 28 dpi, cells/tissue filled about 85% of the NHC-injected injury and around 65% of the PBS- and HA-injected injury (Fig. 2d). The amount of cells/tissue in the injury was significantly higher ($p < 0.05$) with NHC compared with H-210 (Fig. 2d). To clearly visualize the nervous tissue inside the lesion site, we have also performed the Nissl staining as shown in Fig. S2. All of these results confirmed our expectations that NHC provides mechanical strength to a contused spinal cord segment while facilitating cell infiltration and tissue formation.

3.3. Inflammation in the injury

The inflammatory response in an injury is critical for tissue regeneration and repair [31, 32]. We examined macrophage presence and polarization in the injury and in the surrounding tissue at 28 dpi. Macrophages were present in the spinal cords in all groups and among them were pro-regenerative (M2) and pro-inflammatory (M1) macrophage phenotypes (Fig. 3a). The size of the different populations in the damaged spinal cord segment was similar between groups (Fig. 3b). In the tissue outside the injury, the M2/M1 macrophage ratio was largely similar between groups (Fig. 3c). In the injury, the M2/M1 ratio was 4.20 ± 2.30 with NHC, 1.33 ± 0.37 with H-210, 0.61 ± 0.58 with H-80, and 2.70 ± 2.13 with PBS (Fig. 3c). The M2/M1 ratio in the injury was significantly greater ($p < 0.05$) in rats with NHC compared with H-80 (Fig. 3c). Our results indicate that NHC facilitates polarization towards the M2 pro-regenerative phenotype among the infiltrated macrophages.

Cross-sectional segments were used to visualize the potential interaction between PCL fibers and macrophages within the injury. M2, but not M1, macrophages appeared to congregate in nanofiber-rich areas (Fig. 4a). In the spinal cords injected with HA only, M2 and M1 macrophages were intermingled throughout the injury (Figs. 4b, 4c). These observations warrant further investigations into the modulatory interactions between nanofibers and macrophages.

3.4. Vascularization in the injury

Vascularization is important for repair, maintenance, and functioning of tissues. Blood vessels were present in the injury in spinal cords in all groups at 3 (Fig. 5a), 7 (Fig. 5b), and 28 (Fig. 5c) dpi. The blood vessel density increased in time in the injury with NHC or HA but decreased in the injury with PBS (Fig. 5d). At 28 dpi, the density of blood vessels in the injury was 414.1 ± 192.5 when injected with NHC, 341.4 ± 126.5 with H-210, 369.4 ± 55.8 with H-80, and 79.1 ± 20.5 with PBS (Fig. 5d). The blood vessel density was significantly higher ($p < 0.05$) in spinal cords injected with H-80 than with PBS (Fig. 5d). These results suggest that NHC or HA can support angiogenesis and/or maintenance of new vessels in the tissue within the injury.

3.5. Axons in the injury

Axonal growth in the injured spinal cord is important for spinal cord repair. We found axons in the injury in spinal cords in all groups at 3 (Fig. 6a), 7 (Fig. 6b), and 28 (Fig. 6c) dpi. The axon density gradually increased in time in the injury injected with NHC or H-210, but not with PBS or H-80 (Fig. 6d). The axon density in the injury at 28 dpi was 368.0 ± 52.4 with the composite, 279.7 ± 48.0 with H-210, 188.1 ± 54.6 with H-80, and 154.7 ± 122.5 with

PBS (Fig. 6d). At this this time point, axon density in the injury with NHC was significantly higher ($p < 0.05$) than with PBS or H-80 (Fig. 6d). Some of the axons in the injury in all groups were closely associated with astrocytes (Fig. 6e).

3.6 Neural-like cells in the injury

The presence of neural-like cells in the injury was examined using antibodies against βIII-tubulin (Tuj1) for immature neurons and doublecortin (DCX) for neuronal stem/progenitor cells. Tuj1-positive cells were found in the injury in spinal cords in all groups at 3 (Fig. 7a), 7 (Fig. 7b), and 28 (Fig. 7c) dpi. At 28 dpi, Tuj1-positive neurites in the injury with NHC appeared longer and more continuous than those in the other groups (Fig. 7c). Quantitative analysis at 28 dpi revealed that the number of Tuj1-positive cells in the injury was 215.51 ± 70.03 with the composite, 122.74 ± 17.80 with H-210, 103.07 ± 60.21 with H-80, and 82.51 ± 33.56 with PBS. The number of Tuj1-positive cells in the injury with PBS, H-80, or H-210 at 28 dpi increased during the first week post-injection and remained similar or decreased thereafter (Fig. 7d). In contrast, with the composite, the number of Tuj1-positive cells were maintained or increased from 7 to 28 dpi (Fig. 7d). At 28 dpi, the number of Tuj1-positive cells in the injury with the composite was significantly higher ($p < 0.01$) than that with PBS (Fig. 7d). DCX-positive cells were located along the outer border of the injury in all groups (Fig. 7e). In the composite-injected group, DCX positive cells were also readily found in the composite (Fig. 7e). Our findings suggest that NHC facilitated an environment compatible with neurogenesis both in the injury and the surrounding spinal cord nervous tissue.

4. Discussion

4.1. Functionality of the composite

The contused spinal cord gradually decreases in width at the site of impact due to the loss of nervous tissue [33, 34]. We showed that our injectable composite of a HA hydrogel with interfacial bound PCL nanofibers, to increase its mechanical strength to a G' of 210 Pa [18, 19] but maintain adequate porosity [8, 20, 30], limits spinal cord thinning and facilitates cell infiltration and the formation of cellular structures compared with controls. We found that our composite had a similar fibrillary microarchitecture as native spinal cord ECM and resulted in 85% of the injury occupied by cells and structures. HA hydrogel only with a G' of 210 Pa, similar as NHC, but not HA hydrogel with a G' of 80 Pa, limited spinal cord thinning compared with controls, as we expected. However, though both similarly limited spinal cord thinning, the volume of tissue in the injury with HA hydrogel (G' = 210 Pa) was significantly smaller compared with NHC. Thus, the loss in porosity by increasing mechanical strength of HA hydrogel through increasing the concentration negatively affects cell infiltration, which supports the use of interfacial bonding with PCL nanofibers. The finding that NHC facilitated cell infiltration and tissue formation corroborate earlier data obtained with subcutaneously applied NHC [20].

HA enzymatically degrades by hyaluronidase, while PCL degrades through bulk hydrolysis [20]. PCL fibers could last up to 18 months *in vivo*. The interfacial bonding of the PCL fibers to the HA hydrogel contributes to a more homogenous distribution of the fibers throughout the composite. On the other hand, the bonding limits degradation studies because

without it obtaining a mixture with properly distributed fibers inside the hydrogel matrix, which is needed for degradation studies, is difficult [20].

Our data substantiated that NHC satisfied our preset engineering goals to limit spinal cord collapse and provide a microenvironment conducive for cell infiltration and tissue formation. The precise roles of PCL fibers and interfacial bonding in providing these specific characteristics to our composite remain subject for investigation.

4.2. Inflammation shift

A shift in the macrophage population in a contusion from a pro-inflammatory, M1 phenotype to a pro-regenerative, M2 phenotype [32, 35, 36] contributes to repair [32, 35, 37, 38]. We found that NHC facilitated such a pro-repair phenotype shift among macrophages in, but not outside, the injury. In fact, we found on average 2.5 times more M2 macrophages in the injury with NHC compared to the other experimental groups, while the total number of macrophages was similar between the groups. Interestingly, our results suggested that this phenotype shift in NHC was associated with PCL fibers. We found M2 macrophages predominantly in the areas with the fibers, while M1 and M2 macrophages were similarly dispersed in areas with HA only in the injury injected with NHC or HA hydrogel. The possible modulatory role of the PCL fibers in macrophage phenotype shift warrant further investigation. Previously, it was shown that fiber thickness [44] and their physical guidance [45, 46] could stimulate the shift in macrophage phenotype. In general, the stiffness of a material may influence the phenotype of macrophages [39]. For instance, chitosan [40], collagen [41], decellularized ECM [42], and HA [43] were all shown to influence macrophage phenotype shift.

4.3. Vascularization

New blood vessel formation in the contused spinal cord is limited [31, 47]. With NHC, the number of blood vessels in the injury increased over time to more than 5 times the amount in controls at 28 dpi, indicating that NHC facilitated angiogenesis within the contused spinal cord segment. Also, blood vessels were larger and longer with NHC compared with controls, suggesting maturation of the newly formed blood vessels. With HA hydrogel only, we also found an increase in the number of blood vessels in the injury, which corroborates earlier evidence of the innate angiogenic properties of HA [48, 49. 50, 51]. The degree of vascularization in the injury with NHC or HA hydrogel was similar; which makes it unlikely that the PCL fibers played a role in the angiogenic response.

Previously, we discussed possible mechanisms of NHC-mediated angiogenesis and tissue remodeling, with a focus on the local inflammatory response [20]. The porous nature of the composite allows infiltration of host monocytes and macrophages. The PCL fibers may have a role in macrophage polarization into a pro-regenerative M2 phenotype. M2 macrophages are known for producing angiogenic factors, such as vascular endothelial growth factor-D, and tissue remodeling factors, such as chemokine (C-C motif) ligand 2 or matrix metallopeptidase 9, which may mediate further recruitment of macrophages and endothelial progenitors to facilitate angiogenesis. A proteomic analysis of the contusion

in time after injury/injection would increase our insight in the molecular underpinnings of NHC-mediated blood vessel formation.

Our data shows that NHC facilitates the formation of new blood vessels, which is highly likely to support nervous tissue repair and regeneration.

4.4. Neurogenesis

In the contused spinal cord, neural stem cells derive from the ependymal layer [52, 53]. With NHC, we found a significant 2.6-fold increase in immature neurons in the injury compared with controls. With HA only, the number of immature neurons in the injury was not significantly different from that in controls nor with NHC. Little is known about the effects of HA on the fate of endogenous neural stem cells *in vivo*. HA has been used to deliver stem cells to a variety of tissues [54]. We showed here that the number of immature neurons increased during the 4 week survival time only with NHC, suggesting that the gradually changing microenvironment of the NHC-containing injury supported the differentiation of endogenous stem cells into immature neurons and their survival. It is possible that the shift in the macrophage population towards a pro-regenerative, M2 phenotype and the angiogenesis that both occur in the injury with NHC contribute to *de novo* neural tissue formation. Further investigations could increase our understanding of the potential of NHC to generate new nervous tissue.

In the contused spinal cord, growth of severed axons is limited [33]. With NHC, the number of axons in the injury gradually increased over time to more than twice the number in controls at 28 dpi. Other hydrogels were reported to promote and/or facilitate axonal growth in damaged nervous tissue in a variety of injury models [11, 12]. Some axons may derive from the immature neurons present in the injury, but it is possible that NHC provided a growth conducive environment for spinal cord axons. There was no significant increase in axon presence in the injury with HA only, which corroborates *in vitro* findings that HA does not promote neurite growth [55].

4.5. Significance of our injectable composite

There are several aspects of NHC that underline its significance. First, NHC is an injectable material which facilitates treatment of closed injuries such as a contusion, the prevalent mechanism of a SCI in humans. Typically, a contused spinal cord segment collapses in time due to the loss of nervous tissue. To address this problem, we mixed PCL nanofibers into the HA hydrogel which enables to manufacture a composite with a G' in the range of that of spinal cord nervous tissue to provide physical support to the contusion. In previous studies using HA-based, peptide-based, or other types of injectable scaffolds, the spinal cord in the injured segment collapsed [13, 63] or was poorly filled by cells and issue leaving large cystic cavities [58]. The PCL fibers and the HA hydrogel in our composite were mixed using interfacial bonding which allows to maintain a porosity similar as that of HA hydrogel with a G' of 100 Pa. Our results showed that this approach facilitates invasion of cells and formation of cellular structures, which is crucial for tissue repair and *de novo* generation.

To our knowledge, NHC is the first reported injectable hydrogel that within a SCI directs macrophage polarization towards an M2 phenotype, which is known to support nervous

tissue repair. Previous research showed that injectable HA-based hydrogels can elicit axon responses accompanied by improvements in functional recovery [59, 60]. However, in these studies with injectable HA-based hydrogels, as well as studies using solid HA-based scaffolds [56–58], a shift among macrophages towards the M2 phenotype was not reported. Non-HA-based scaffolds have also been examined for their potential to repair tissue [61, 62], but none was reported to direct macrophage polarization. The finding that NHC directs a shift among macrophages towards the M2 phenotype in the injured spinal cord is a significant property of our composite.

NHC elicits significant repair effects itself without any added repair-supporting biologics. So far, different types of injectable materials have been used to deliver repair-supporting cells and/or growth factors to the injured spinal cord which resulted in variable success in repair and recovery [64, 65, 66]. However, from these studies it was clear that the injectable material on its own did not result in tissue repair or generation. We now report that NHC itself elicits significant repair-supporting events leading to the invasion of cells and the formation of new structures in the injury site. In future studies, NHC could be used in combination with cells and growth factors to maximize the repair effects.

5. Conclusions

This engineered PCL nanofiber-HA hydrogel composite with interfacial bonding provided mechanical support to the contused spinal cord and promoted a shift towards a pro-regenerative macrophage population, angiogenesis, neurogenesis, and axon presence. The reparative effects of NHC in the contused spinal cord have been summarized in Figure 8. At present, the interplay between macrophages, blood vessels, neural stem cells, and axons is acknowledged but incompletely understood. The shift in macrophage polarization towards the M2 phenotype likely supported the formation of new blood vessels [31], thereby creating a conducive environment for neurogenesis and axonal growth. The precise roles of the PCL nanofibers in the NHC-mediated cellular events need further investigations. Our present data suggest an active role in creating a pro-regenerative environment through stimulation of macrophage polarization. NHC treatment has clear reparative potential, including stimulation of *de novo* neural tissue formation and axonal growth; however, this did not translate into functional recovery in our SCI model. Conceivably, using NHC as a transplant medium for repair-supporting cells such as mesenchymal stromal cells or Schwann cells could combine the benefits of both reparative approaches. These properties of the composite suggest its strong translational potential for treating the injured spinal cord.

Supplementary Material

Refer to Web version on PubMed Central for supplementary material.

Acknowledgements

This work was supported by the U.S. National Institute of Neurological Disorders and Stroke (R21NS085714 to H.-Q.M.), Coulter Foundation Translational Grant (H.-Q.M.), the Cohen Translational Engineering Fund (H.-Q.M.), Louis B. Thalheimer Award for Translational Research (H.-Q.M.), the Abell Foundation Translational Award (H.-Q.M.), the National Institutes of Health (NS101298 to M.O.), Craig H. Neilsen Foundation (460461 to M.O.), and

The Department of Veterans Affairs (I01RX001807 to M.O.). X.L. acknowledges the AHA Career Development Award (18CDA34110314).

References

[1]. Spinal Cord Injury Facts and Figures at a Glance, The journal of spinal cord medicine 35(1) 68–69. [PubMed: 22330194]

[2]. Yao S, Yu S, Cao Z, Yang Y, Yu X, Mao HQ, Wang LN, Sun X, Zhao L, Wang X, Hierarchically aligned fibrin nanofiber hydrogel accelerated axonal regrowth and locomotor function recovery in rat spinal cord injury, Int J Nanomedicine 13 (2018) 2883–2895. [PubMed: 29844671]

[3]. McCreedy DA, Sakiyama-Elbert SE, Combination therapies in the CNS: engineering the environment, Neurosci Lett 519(2) (2012) 115–21. [PubMed: 22343313]

[4]. Khaing ZZ, Thomas RC, Geissler SA, Schmidt CE, Advanced biomaterials for repairing the nervous system: what can hydrogels do for the brain?, Materials Today 17(7) (2014) 332–340.

[5]. Park J, Lim E, Back S, Na H, Park Y, Sun K, Nerve regeneration following spinal cord injury using matrix metalloproteinase-sensitive, hyaluronic acid-based biomimetic hydrogel scaffold containing brain-derived neurotrophic factor, Journal of Biomedical Materials Research Part A 93A(3) (2010) 1091–1099.

[6]. Chen J, Zhang Z, Liu J, Zhou R, Zheng X, Chen T, Wang L, Huang M, Yang C, Li Z, Yang C, Bai X, Jin D, Acellular spinal cord scaffold seeded with bone marrow stromal cells protects tissue and promotes functional recovery in spinal cord-injured rats, Journal of neuroscience research 92(3) (2014) 307–17. [PubMed: 24375695]

[7]. Li XW, Katsanevakis E, Liu XY, Zhang N, Wen XJ, Engineering neural stem cell fates with hydrogel design for central nervous system regeneration, Progress in Polymer Science 37(8) (2012) 1105–1129.

[8]. Li X, Liu X, Zhang N, Wen X, Engineering in situ cross-linkable and neurocompatible hydrogels, Journal of neurotrauma 31(16) (2014) 1431–1438. [PubMed: 24447305]

[9]. Straley KS, Foo CWP, Heilshorn SC, Biomaterial Design Strategies for the Treatment of Spinal Cord Injuries, Journal of neurotrauma 27(1) (2010) 1–19. [PubMed: 19698073]

[10]. Baumann MD, Kang CE, Tator CH, Shoichet MS, Intrathecal delivery of a polymeric nanocomposite hydrogel after spinal cord injury, Biomaterials 31(30) (2010) 7631–9. [PubMed: 20656347]

[11]. Cigognini D, Satta A, Colleoni B, Silva D, Donega M, Antonini S, Gelain F, Evaluation of early and late effects into the acute spinal cord injury of an injectable functionalized self-assembling scaffold, PloS one 6(5) (2011) e19782.

[12]. Tysseling-Mattiace VM, Sahni V, Niece KL, Birch D, Czeisler C, Fehlings MG, Stupp SI, Kessler JA, Self-assembling nanofibers inhibit glial scar formation and promote axon elongation after spinal cord injury, J Neurosci 28(14) (2008) 3814–23. [PubMed: 18385339]

[13]. Hong LTA, Kim YM, Park HH, Hwang DH, Cui Y, Lee EM, Yahn S, Lee JK, Song SC, Kim BG, An injectable hydrogel enhances tissue repair after spinal cord injury by promoting extracellular matrix remodeling, Nat Commun 8(1) (2017) 533. [PubMed: 28912446]

[14]. Pertici V, Amendola J, Laurin J, Gigmes D, Madaschi L, Carelli S, Marqueste T, Gorio A, Decherchi P, The use of poly(N-[2-hydroxypropyl]-methacrylamide) hydrogel to repair a T10 spinal cord hemisection in rat: a behavioural, electrophysiological and anatomical examination, ASN Neuro 5(2) (2013) 149–66. [PubMed: 23614684]

[15]. Kubinova S, Horak D, Hejcl A, Plichta Z, Kotek J, Proks V, Forostyak S, Sykova E, SIKVAV-modified highly superporous PHEMA scaffolds with oriented pores for spinal cord injury repair, Journal of tissue engineering and regenerative medicine 9(11) (2015) 1298–309. [PubMed: 23401421]

[16]. Tsai EC, Dalton PD, Shoichet MS, Tator CH, Synthetic hydrogel guidance channels facilitate regeneration of adult rat brainstem motor axons after complete spinal cord transection, Journal of neurotrauma 21(6) (2004) 789–804. [PubMed: 15253805]

[17]. Bakshi A, Fisher O, Dagci T, Himes BT, Fischer I, Lowman A, Mechanically engineered hydrogel scaffolds for axonal growth and angiogenesis after transplantation in spinal cord injury, Journal of Neurosurgery-Spine 1(3) (2004) 322–329. [PubMed: 15478371]

[18]. Ozawa H, Matsumoto T, Ohashi T, Sato M, Kokubun S, Comparison of spinal cord gray matter and white matter softness: measurement by pipette aspiration method, J Neurosurg 95(2 Suppl) (2001) 221–4. [PubMed: 11599840]

[19]. Ware T, Simon D, Arreaga-Salas DE, Reeder J, Rennaker R, Keefer EW, Voit W, Fabrication of Responsive, Softening Neural Interfaces, Advanced Functional Materials 22(16) (2012) 3470–3479.

[20]. Li X, Cho B, Martin R, Seu M, Zhang C, Zhou Z, Choi JS, Jiang X, Chen L, Walia G, Yan J, Callanan M, Liu H, Colbert K, Morrissette-McAlmon J, Grayson W, Reddy S, Sacks JM, Mao HQ, Nanofiber-hydrogel composite-mediated angiogenesis for soft tissue reconstruction, Sci Transl Med 11(490) (2019).

[21]. Wang L, Wu Y, Guo B, Ma P, Nanofiber Yarn/Hydrogel Core-Shell Scaffolds Mimicking Native Skeletal Muscle Tissue for Guiding 3D Myoblast Alignment, Elongation, and Differentiation, Acs Nano 9(9) (2015) 9167–9179. [PubMed: 26280983]

[22]. Wang TY, Bruggeman KF, Kauhausen JA, Rodriguez AL, Nisbet DR, Parish CL, Functionalized composite scaffolds improve the engraftment of transplanted dopaminergic progenitors in a mouse model of Parkinson's disease, Biomaterials 74 (2016) 89–98. [PubMed: 26454047]

[23]. Jiang X, Christopherson GT, Mao HQ, The effect of nanofibre surface amine density and conjugate structure on the adhesion and proliferation of human haematopoietic progenitor cells, Interface Focus 1(5) (2011) 725–33. [PubMed: 23050077]

[24]. Rauck BM, Novosat TL, Oudega M, Wang Y, Biocompatibility of a coacervate-based controlled release system for protein delivery to the injured spinal cord, Acta Biomaterialia 11 (2015) 204–211. [PubMed: 25266504]

[25]. Ritfeld GJ, Rauck BM, Novosat TL, Park D, Patel P, Roos RAC, Wang Y, Oudega M, The effect of a polyurethane-based reverse thermal gel on bone marrow stromal cell transplant survival and spinal cord repair, Biomaterials 35(6) (2014) 1924–1931. [PubMed: 24331711]

[26]. Basso DM, Beattie MS, Bresnahan JC, A sensitive and reliable locomotor rating scale for open field testing in rats, Journal of neurotrauma 12(1) (1995) 1–21. [PubMed: 7783230]

[27]. Zou J, Liu S, Sun J, Yang W, Xu Y, Rao Z, Jiang B, Zhu Q, Liu X, Wu J, Chang C, Mao H, Ling E, Quan D, Zeng Y, Peripheral Nerve-Derived Matrix Hydrogel Promotes Remyelination and Inhibits Synapse Formation, Advanced Functional Materials 28(13) (2018).

[28]. Li X, Tzeng SY, Liu X, Tammia M, Cheng Y-H, Rolfe A, Sun D, Zhang N, Green JJ, Wen X, Mao H-Q, Nanoparticle-mediated transcriptional modification enhances neuronal differentiation of human neural stem cells following transplantation in rat brain, Biomaterials 84 (2016) 157–166. [PubMed: 26828681]

[29]. Kunkel-Bagden E, Dai HN, Bregman BS, Recovery of function after spinal cord hemisection in newborn and adult rats: differential effects on reflex and locomotor function, Experimental neurology 116(1) (1992) 40–51. [PubMed: 1559563]

[30]. Li X, Liu X, Josey B, Chou CJ, Tan Y, Zhang N, Wen X, Short laminin peptide for improved neural stem cell growth, Stem Cells Translational Medicine 3(5) (2014) 662–670. [PubMed: 24692587]

[31]. Haggerty AE, Maldonado-Lasuncion I, Oudega M, Biomaterials for revascularization and immunomodulation after spinal cord injury, Biomed Mater 13(4) (2018) 044105.

[32]. Maldonado-Lasuncion I, Verhaagen J, Oudega M, Mesenchymal Stem Cell-Macrophage Choreography Supporting Spinal Cord Repair, Neurotherapeutics 15(3) (2018) 578–587. [PubMed: 29728851]

[33]. Hagg T, Oudega M, Degenerative and spontaneous regenerative processes after spinal cord injury, Journal of neurotrauma 23(3–4) (2006) 264–80. [PubMed: 16629615]

[34]. Kwon BK, Tetzlaff W, Spinal cord regeneration: from gene to transplants, Spine 26(24 Suppl) (2001) S13–22. [PubMed: 11805602]

[35]. Gensel JC, Zhang B, Macrophage activation and its role in repair and pathology after spinal cord injury, Brain Res 1619 (2015) 1–11. [PubMed: 25578260]

[36]. Kigerl KA, Gensel JC, Ankeny DP, Alexander JK, Donnelly DJ, Popovich PG, Identification of two distinct macrophage subsets with divergent effects causing either neurotoxicity or regeneration in the injured mouse spinal cord, J Neurosci 29(43) (2009) 13435–44.

[37]. Blight AR, Macrophages and inflammatory damage in spinal cord injury, Journal of neurotrauma 9 Suppl 1 (1992) S83–91. [PubMed: 1588634]

[38]. Popovich PG, Guan Z, McGaughy V, Fisher L, Hickey WF, Basso DM, The neuropathological and behavioral consequences of intraspinal microglial/macrophage activation, J Neuropathol Exp Neurol 61(7) (2002) 623–33. [PubMed: 12125741]

[39]. McWhorter FY, Davis CT, Liu WF, Physical and mechanical regulation of macrophage phenotype and function, Cell Mol Life Sci 72(7) (2015) 1303–16. [PubMed: 25504084]

[40]. Chedly J, Soares S, Montembault A, von Boxberg Y, Veron-Ravaille M, Mouffle C, Benassy MN, Taxi J, David L, Nothias F, Physical chitosan microhydrogels as scaffolds for spinal cord injury restoration and axon regeneration, Biomaterials 138 (2017) 91–107. [PubMed: 28554011]

[41]. Peng Z, Gao W, Yue B, Jiang J, Gu Y, Dai J, Chen L, Shi Q, Promotion of neurological recovery in rat spinal cord injury by mesenchymal stem cells loaded on nerve-guided collagen scaffold through increasing alternatively activated macrophage polarization, Journal of tissue engineering and regenerative medicine 12(3) (2018) e1725-e1736.

[42]. Brown BN, Valentin JE, Stewart-Akers AM, McCabe GP, Badylak SF, Macrophage phenotype and remodeling outcomes in response to biologic scaffolds with and without a cellular component, Biomaterials 30(8) (2009) 1482–91. [PubMed: 19121538]

[43]. Rayahin JE, Buhrman JS, Zhang Y, Koh TJ, Gemeinhart RA, High and low molecular weight hyaluronic acid differentially influence macrophage activation, ACS Biomater Sci Eng 1(7) 481–493. [PubMed: 26280020]

[44]. Wang Z, Cui Y, Wang J, Yang X, Wu Y, Wang K, Gao X, Li D, Li Y, Zheng XL, Zhu Y, Kong D, Zhao Q, The effect of thick fibers and large pores of electrospun poly(epsilon-caprolactone) vascular grafts on macrophage polarization and arterial regeneration, Biomaterials 35(22) (2014) 5700–10. [PubMed: 24746961]

[45]. Teixeira A, Abrams G, Bertics P, Murphy C, Nealey P, Epithelial contact guidance on well-defined micro- and nanostructured substrates, Journal of Cell Science 116(10) (2003) 1881–1892. [PubMed: 12692189]

[46]. McWhorter FY, Wang T, Nguyen P, Chung T, Liu WF, Modulation of macrophage phenotype by cell shape, Proceedings of the National Academy of Sciences of the United States of America 110(43) (2013) 17253–8. [PubMed: 24101477]

[47]. Casella GT, Marcillo A, Bunge MB, Wood PM, New vascular tissue rapidly replaces neural parenchyma and vessels destroyed by a contusion injury to the rat spinal cord, Experimental neurology 173(1) (2002) 63–76. [PubMed: 11771939]

[48]. West DC, Hampson IN, Arnold F, Kumar S, Angiogenesis induced by degradation products of hyaluronic acid, Science 228(4705) (1985) 1324–6. [PubMed: 2408340]

[49]. Baier Leach J, Bivens KA, Patrick CW Jr., Schmidt CE, Photocrosslinked hyaluronic acid hydrogels: natural, biodegradable tissue engineering scaffolds, Biotechnol Bioeng 82(5) (2003) 578–89. [PubMed: 12652481]

[50]. Kang CE, Baumann MD, Tator CH, Shoichet MS, Localized and sustained delivery of fibroblast growth factor-2 from a nanoparticle-hydrogel composite for treatment of spinal cord injury, Cells Tissues Organs 197(1) (2013) 55–63. [PubMed: 22796886]

[51]. Wen Y, Yu S, Wu Y, Ju R, Wang H, Liu Y, Wang Y, Xu Q, Spinal cord injury repair by implantation of structured hyaluronic acid scaffold with PLGA microspheres in the rat, Cell Tissue Res 364(1) (2016) 17–28. [PubMed: 26463048]

[52]. Sabelstrom H, Stenudd M, Frisen J, Neural stem cells in the adult spinal cord, Experimental neurology 260 (2014) 44–9. [PubMed: 23376590]

[53]. Stenudd M, Sabelstrom H, Frisen J, Role of endogenous neural stem cells in spinal cord injury and repair, JAMA Neurol 72(2) (2015) 235–7. [PubMed: 25531583]

[54]. Wu S, Xu R, Duan B, Jiang P, Three-Dimensional Hyaluronic Acid Hydrogel-Based Models for In Vitro Human iPSC-Derived NPC Culture and Differentiation, J Mater Chem B 5(21) (2017) 3870–3878. [PubMed: 28775848]

[55]. Chan CC, Roberts CR, Steeves JD, Tetzlaff W, Aggrecan components differentially modulate nerve growth factor-responsive and neurotrophin-3-responsive dorsal root ganglion neurite growth, Journal of neuroscience research 86(3) (2008) 581–92. [PubMed: 17918743]

[56]. Wei YT, He Y, Xu CL, Wang Y, Liu BF, Wang XM, Sun XD, Cui FZ, Xu QY, Hyaluronic acid hydrogel modified with nogo-66 receptor antibody and poly-L-lysine to promote axon regrowth after spinal cord injury, J Biomed Mater Res B Appl Biomater 95(1) (2010) 110–7. [PubMed: 20725955]

[57]. Khaing ZZ, Milman BD, Vanscoy JE, Seidlits SK, Grill RJ, Schmidt CE, High molecular weight hyaluronic acid limits astrocyte activation and scar formation after spinal cord injury, Journal of neural engineering 8(4) (2011) 046033.

[58]. Gupta D, Tator CH, Shoichet MS, Fast-gelling injectable blend of hyaluronan and methylcellulose for intrathecal, localized delivery to the injured spinal cord, Biomaterials 27(11) (2006) 2370–9. [PubMed: 16325904]

[59]. Austin JW, Kang CE, Baumann MD, DiDiodato L, Satkunendrarajah K, Wilson JR, Stanisz GJ, Shoichet MS, Fehlings MG, The effects of intrathecal injection of a hyaluronan-based hydrogel on inflammation, scarring and neurobehavioural outcomes in a rat model of severe spinal cord injury associated with arachnoiditis, Biomaterials 33(18) (2012) 4555–64. [PubMed: 22459192]

[60]. Wakao N, Imagama S, Zhang H, Tauchi R, Muramoto A, Natori T, Takeshita S, Ishiguro N, Matsuyama Y, Kadomatsu K, Hyaluronan oligosaccharides promote functional recovery after spinal cord injury in rats, Neurosci Lett 488(3) (2011) 299–304. [PubMed: 21111028]

[61]. Cigognini D, Satta A, Colleoni B, Silva D, Donegà M, Antonini S, Gelain F.J.P.o., Evaluation of early and late effects into the acute spinal cord injury of an injectable functionalized self-assembling scaffold, 6(5) (2011) e19782.

[62]. Perale G, Rossi F, Santoro M, Peviani M, Papa S, Llupi D, Torriani P, Micotti E, Previdi S, Cervo L, Sundstrom E, Boccaccini AR, Masi M, Forloni G, Veglianese P, Multiple drug delivery hydrogel system for spinal cord injury repair strategies, J Control Release 159(2) (2012) 271–80. [PubMed: 22227024]

[63]. Mothe AJ, Tam RY, Zahir T, Tator CH, Shoichet MS, Repair of the injured spinal cord by transplantation of neural stem cells in a hyaluronan-based hydrogel, Biomaterials 34(15) (2013) 3775–83. [PubMed: 23465486]

[64]. Guest JD, Moore SW, Aimetti AA, Kutikov AB, Santamaria AJ, Hofstetter CP, Ropper AE, Theodore N, Ulich TR, Layer RT, Internal decompression of the acutely contused spinal cord: Differential effects of irrigation only versus biodegradable scaffold implantation, Biomaterials 185 (2018) 284–300. [PubMed: 30265898]

[65]. Ritfeld GJ, Rauck BM, Novosat TL, Park D, Patel P, Roos RA, Wang Y, Oudega M, The effect of a polyurethane-based reverse thermal gel on bone marrow stromal cell transplant survival and spinal cord repair, Biomaterials 35(6) (2014) 1924–31. [PubMed: 24331711]

[66]. Wang Q, Zhang H, Xu H, Zhao Y, Li Z, Li J, Wang H, Zhuge D, Guo X, Xu H, Jones S, Li X, Jia X, Xiao J, Novel multi-drug delivery hydrogel using scar-homing liposomes improves spinal cord injury repair, Theranostics 8(16) (2018) 4429–4446. [PubMed: 30214630]

[67]. Wang Q, He Y, Zhao Y, Xie H, Lin Q, He Z, Wang X, Li J, Zhang H, Wang C, Gong F, Li X, Xu H, Ye Q, Xiao J, A Thermosensitive Heparin-Poloxamer Hydrogel Bridges aFGF to Treat Spinal Cord Injury, ACS Appl Mater Interfaces 9(8) (2017) 6725–6745. [PubMed: 28181797]

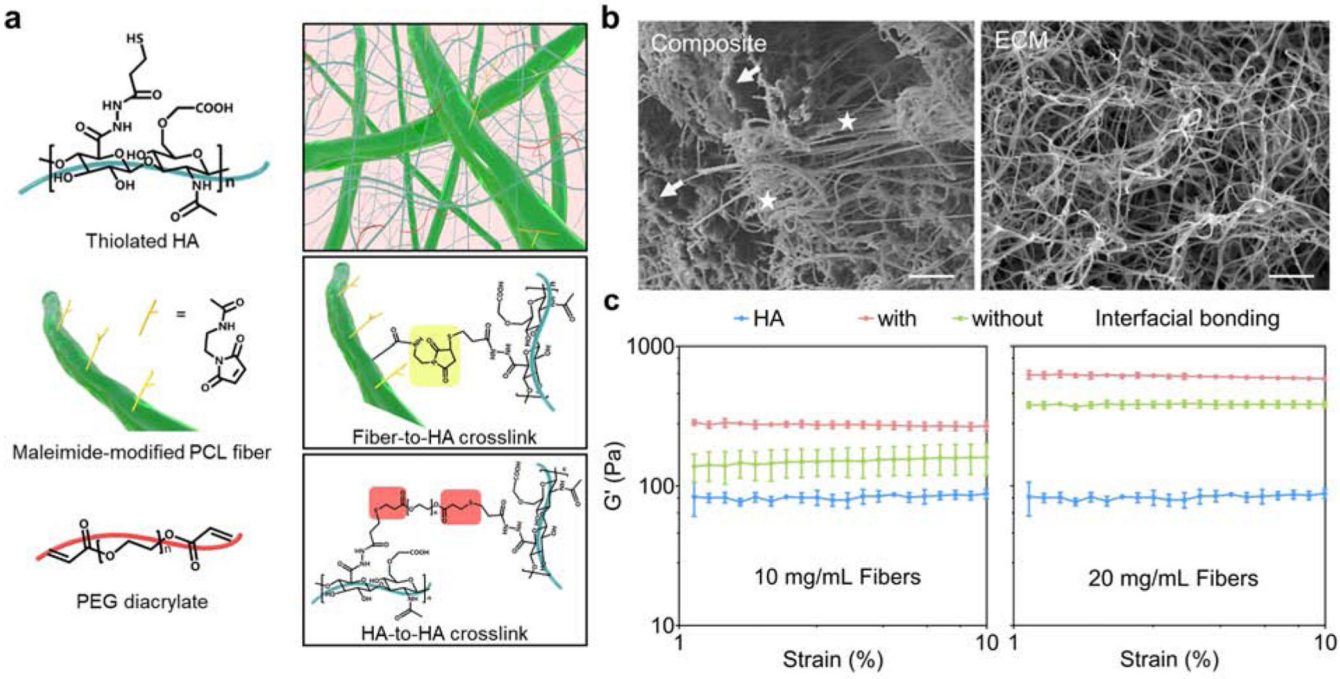

Fig. 1. Engineering a nanofiber-hydrogel composite with interfacial bonding between the fiber surface and hydrogel network.

(**a**) Schematic of the synthesis and structure of the PCL nanofiber-HA hydrogel composite (NHC). (**b**) SEM images of NHC (left), illustrating that PCL fibers (stars) are embedded in the HA hydrogel network (arrows), and porcine native spinal cord ECM (right), revealing the architectural similarity between native ECM and the nanofiber-hydrogel network in general structural features. Scale bars: 2 μm (left) and 10 μm (right). (**c**) Oscillatory strain sweep tests of HA hydrogel and composites with and without interfacial bonding. The fiber-loading amounts were 10 and 20 mg/mL. The HA and PEGDA concentrations were kept at 4 and 2 mg/mL, respectively.

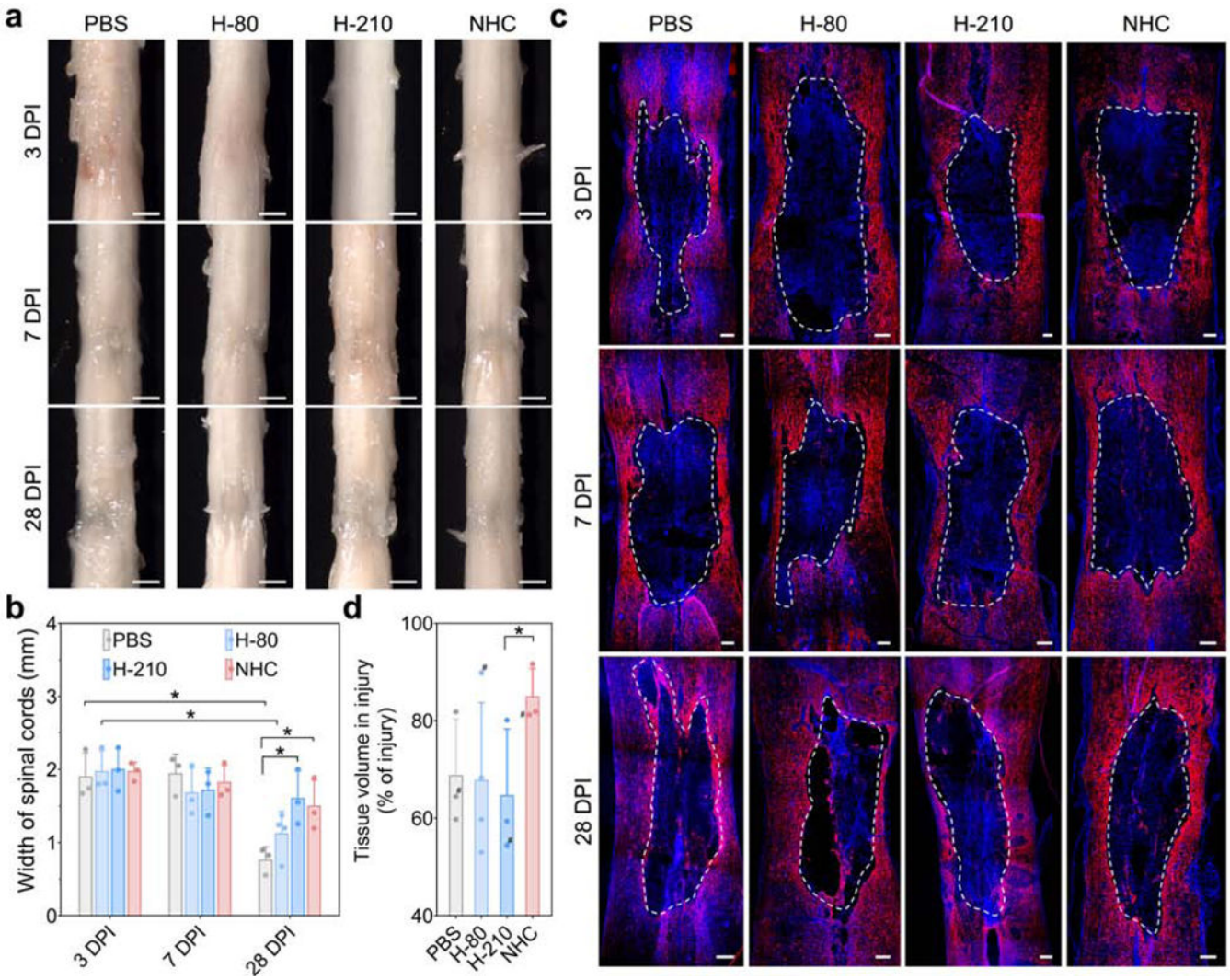

Fig. 2. NHC limits collapse of the contused spinal cord and facilitates tissue formation in the injury.

(**a**) Pictures of representative spinal cords of all treatment groups at 3, 7, and 28 days post-injury (dpi). Scale bar: 1 mm. (**b**) Bar graphs showing the average width of the spinal cords of each treatment group at 3, 7, and 28 dpi (n = 3; * $p < 0.05$). (**c**) Microphotographs of the injury in representative horizontal sections of each of the treatment groups at 3, 7, and 28 dpi. The sections were stained with antibody against glial-fibrillary acidic protein (GFAP, red) to stain astrocytes and counterstained with DAPI (blue). Scale bar: 200 μm. (**d**) Bar graph showing the average volume of tissue in the injury relative to the volume of the injury (% of injury) for each treatment group at 28 dpi (n = 3). Bars represent standard deviation.

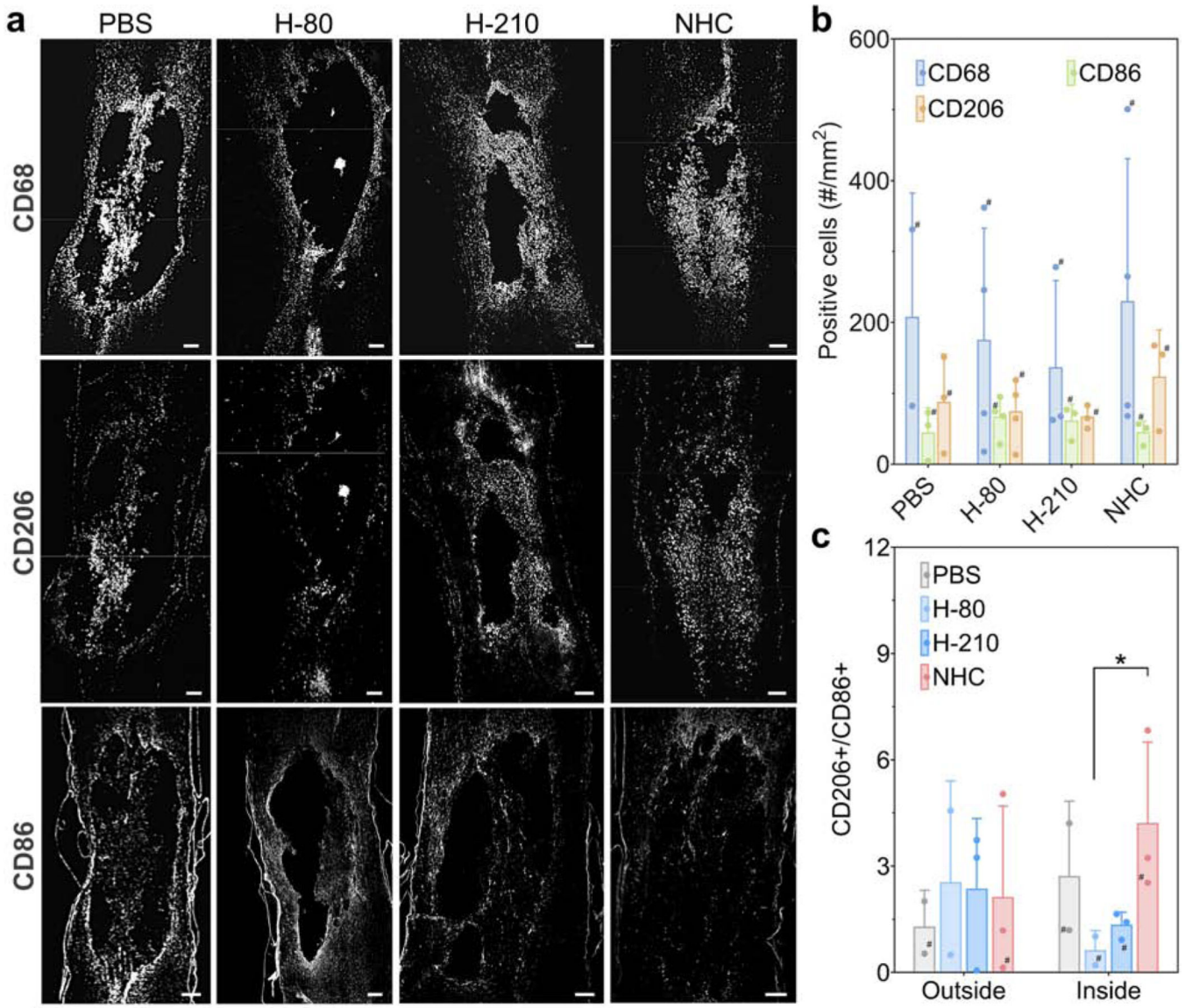

Fig. 3. NHC facilitates a shift among macrophages towards the pre-regenerative phenotype.

(**a**) Microphotographs showing macrophages in and around the injury in representative horizontal sections of the treatment groups at 28 days post-injury (dpi). Scale bar: 200 μm. The sections were stained with antibodies against CD68 to recognize pan-macrophages, CD206 to recognize pro-regenerative macrophages, or CD86 to recognize pro-inflammatory macrophages. (**b**) Bar graph showing the average number of CD68+, CD86+, and CD206+ cells in the injury and surrounding spinal cord of each treatment group at 28 dpi (n = 3). Bars represent standard deviation. (**c**) Bar graph showing the average CD206+/CD86+ ratio in and outside the injury for each of the treatment group at 28 dpi (n = 3; * $p < 0.05$). Bars represent standard deviation.

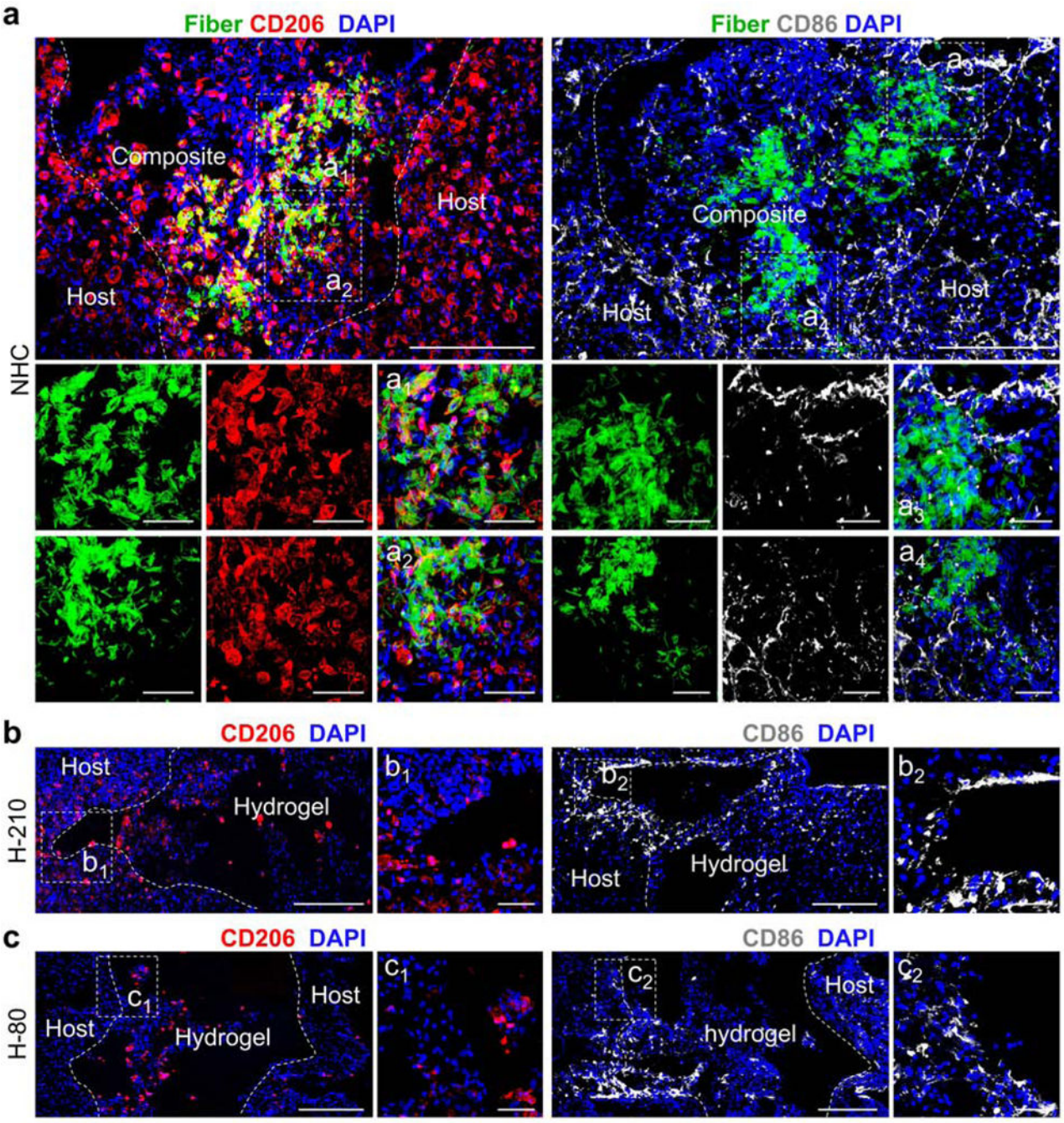

Fig. 4. Pro-regenerative macrophages are present in PCL nanofiber-rich areas in the composite.

Microphotographs of pro-regenerative macrophages, stained with antibodies against CD206 (red), and pro-inflammatory macrophages, stained with antibodies against CD86 (white), in (**a**) NHC, (**b**) H-210, and (**c**) H-80 at 28 days post-injury (dpi). PCL nanofibers fluoresce in green due to F8BT. Sections were counterstained with DAPI (blue). Scale bar: 500 μm. For higher magnification, scale bar represents 100 μm.

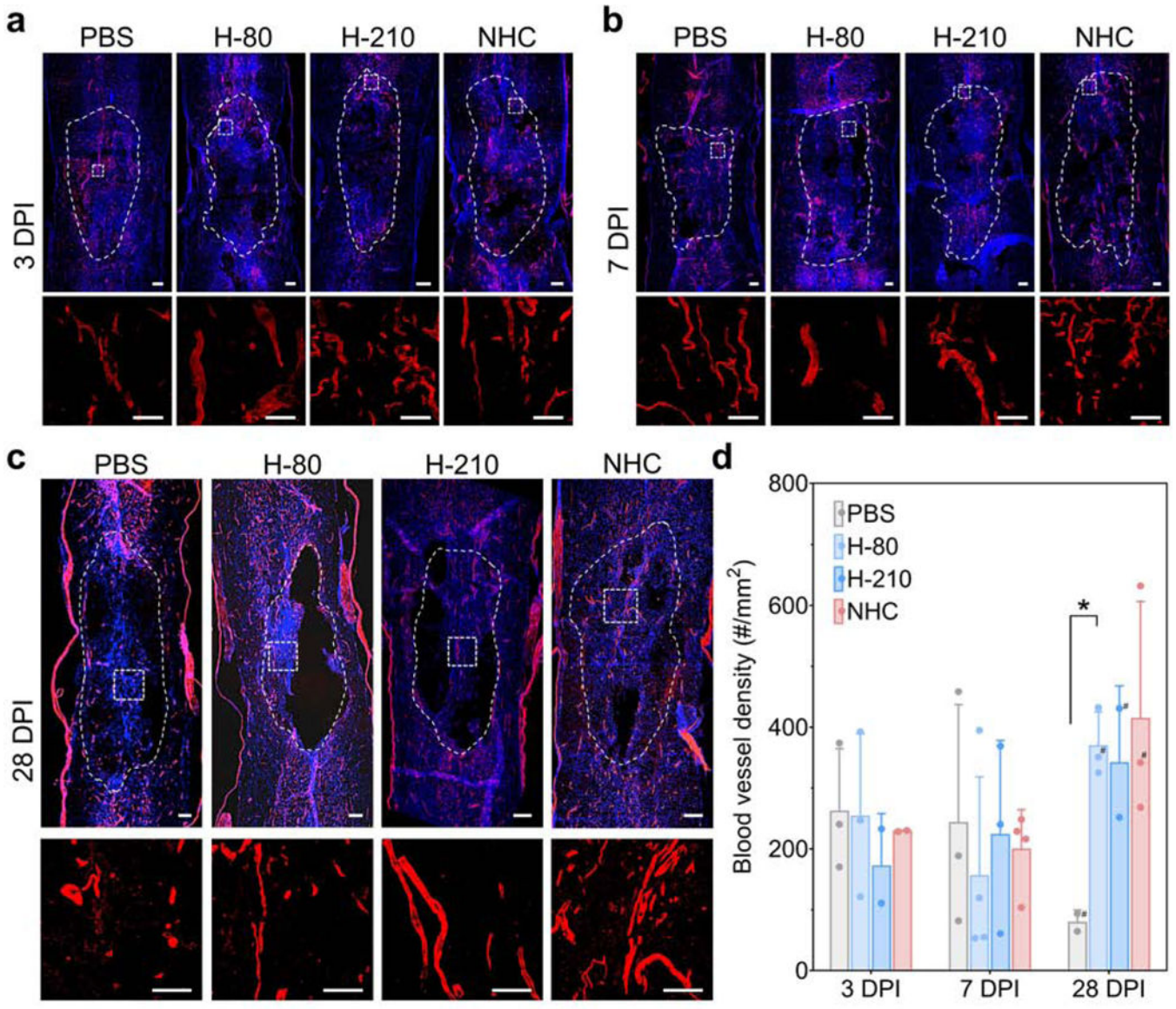

Fig. 5. Blood vessels are present in the NHC-injected injury.

Microphotographs showing blood vessels in the injury in representative horizontal sections of each treatment group at (**a**) 3, (**b**) 7, and (**c**) 28 days post-injury (dpi). Scale bar: 200 μm. Sections were stained with antibodies against RECA-1 to recognize endothelial cells (red) and counterstained with DAPI (blue). The injury is outlined by the dashed line. The higher magnifications show blood vessels in the injury. Scale bar: 100 μm. (**d**) Bar graph showing the average density of blood vessels in the injury (extended 500 μm rostral and caudal beyond the lesion edges) for each treatment group at 3, 7, and 28 dpi (n = 3; * $p <$ 0.05). Bars represent standard deviation.

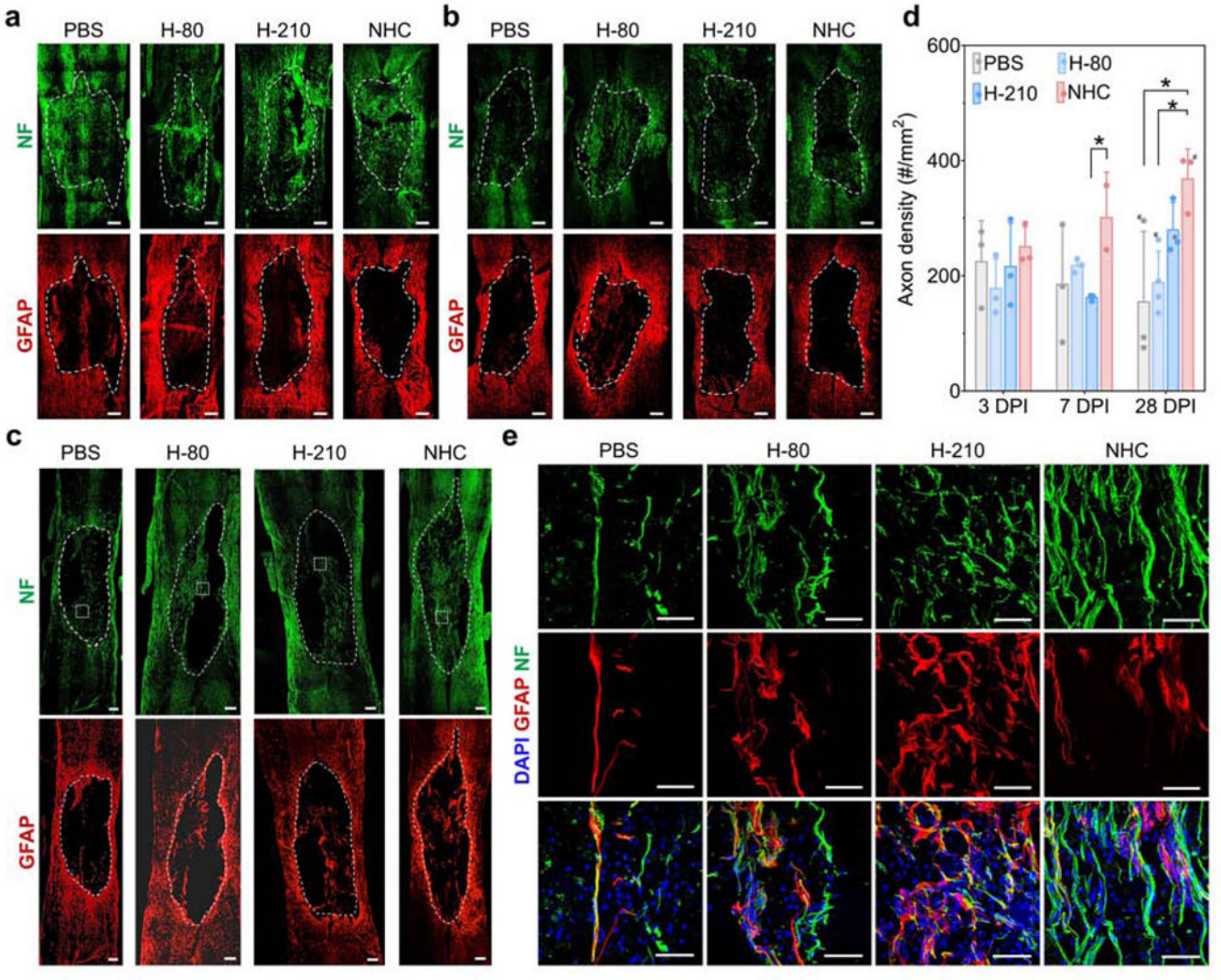

Fig. 6. NHC endorsed axon growth into the injury.

Axons in the injury shown in representative horizontal sections of each treatment group at (**a**) 3, (**b**) 7, and (**c**) 28 days post-injury (dpi). Scale bar: 200 μm. Sections were stained with antibodies against neurofilament (NF, green) to recognize axons and against glial-fibrillary acidic protein (GFAP, red) to recognize reactive astrocytes. Scale bar: 200 μm. (**d**) Bar graph showing the density of axons in the lesion site (extended 500 μm rostrally and caudally beyond the lesion edges) for each treatment group at 3, 7, and 28 dpi (n = 3; * $p < 0.05$). Bars represent standard deviation. (**e**) Higher magnifications of representative area (outlined in **c**) in the injury of each treatment group showing NF (upper row), GFAP (middle row), and DAPI/NF/GFAP (bottom row). Scale bar: 100 μm.

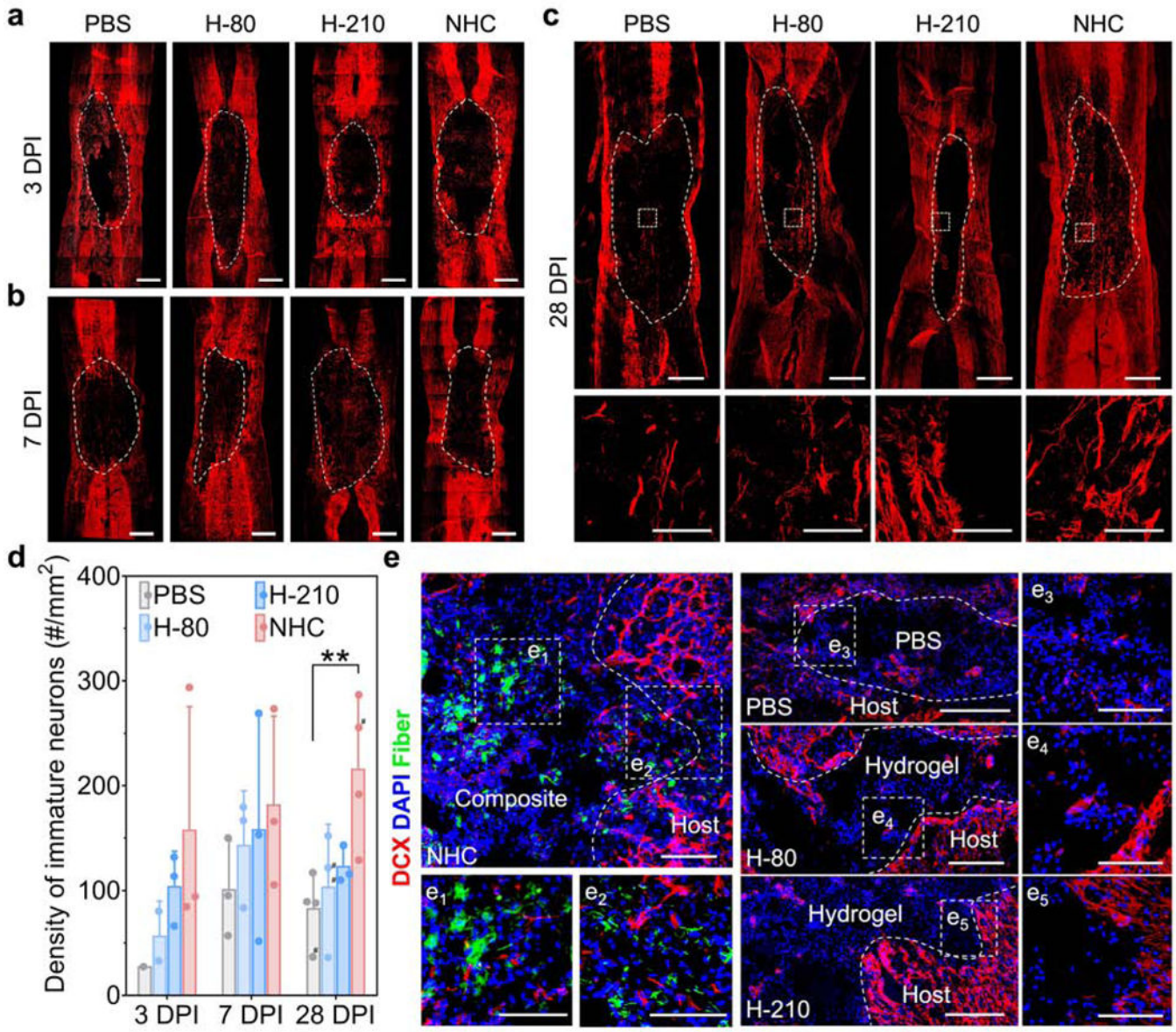

Fig. 7. NHC stimulated neurogenesis in the injury.

Microphotographs showing immature neurons stained with antibodies against βIII-tubulin and around the injury in representative horizontal sections of each treatment group at 3 (**a**), 7 (**b**), and 28 (**c**) days post-injury (dpi). Scale bar: 200 μm. Representative area for each group at 28 dpi is shown in high magnification in **c**. Scale bar: 100 μm. (**d**) Bar graph showing the average density of immature neurons per mm^2 in the injury for each experimental group at 3, 7, and 28 dpi (n = 3; ** $p < 0.01$). Bars represent standard deviation. (**e**) Microphotographs showing neural precursor cells stained with antibodies against doublecortin (DCX, red) in and around the injury in horizontal sections of each treatment group at 28 dpi. PCL fibers fluoresce in green due to F8BT. Sections were counterstained with DAPI (blue). For each group, inserts are depicted in high magnification images. Scale bar: 100 μm.

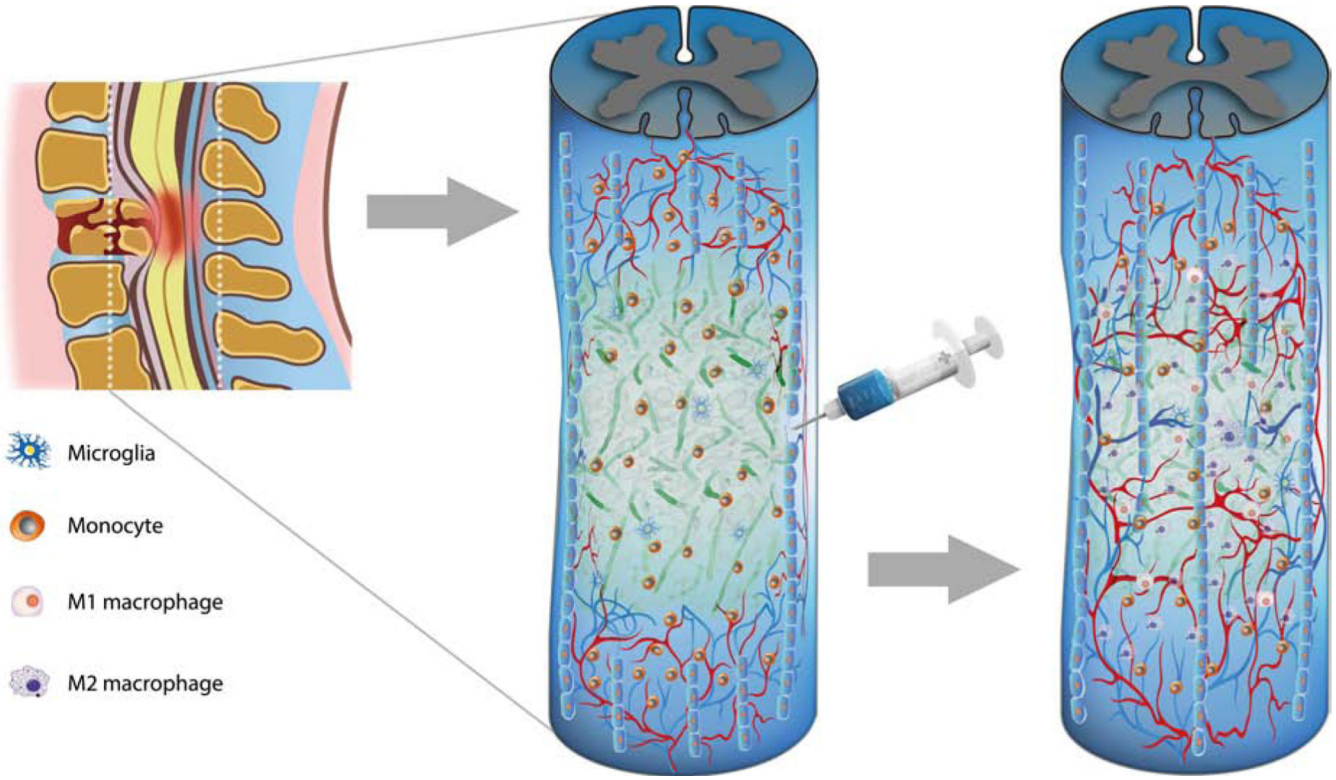

Fig. 8. Schematic representation of the results with NHC in the injury.

Based on our morphological and anatomical evaluation of the spinal cords in our experiment, we demonstrated that a subacute injection of NHC into the contused spinal cord limited the typical collapse of the spinal cord, promoted a shift in macrophage polarization towards a pro-regenerative (M2) phenotype, facilitated cell invasion, and elicited blood vessel formation, axon growth, and neurogenesis. Together, our results support the further investigation of NHC for nervous tissue repair.